

UDC 621.372.2

<https://doi.org/10.33619/2414-2948/103/43>

MODELING OF THE ORGANIC RANKINE CYCLE BASED ON THE THEORY OF ENERGY CHAINS

©**Kireev N.**, ORCID: 0009-0008-0563-317X, Ogarev Mordovia State University, Saransk, Russia, kireev_mdf117@mail.ru

©**Kudashev S.**, ORCID: 0000-0002-9554-9746, SPIN-code: 4763-0003, Ph.D., Ogarev Mordovia State University, Saransk, Russia, kudashev@mail.ru

©**Zhang Qiang**, ORCID: 0000-0002-5092-168X, Dr. habil., Jiangsu University of Science and Technology, Zhenjiang, China, zhangqiang@just.edu.cn

МОДЕЛИРОВАНИЕ ОРГАНИЧЕСКОГО ЦИКЛА РЕНКИНА НА ОСНОВЕ ТЕОРИИ ЭНЕРГЕТИЧЕСКИХ ЦЕПЕЙ

©**Киреев Н. С.**, ORCID: 0009-0008-0563-317X, Национальный исследовательский Мордовский государственный университет им. Н.П. Огарева, Саранск, Россия, kireev_mdf117@mail.ru

©**Кудашев С. Ф.**, SPIN-код: 4763-0003, ORCID: 0000-0002-9554-9746, канд. техн. наук, Национальный исследовательский Мордовский государственный университет им. Н.П. Огарева, Саранск, Россия, kudashev@mail.ru

©**Чжан Цян**, ORCID: 0000-0002-5092-168X, д-р техн. наук, Университет науки и технологии Цзянсу, Чжэньцзян, Китай, zhangqiang@just.edu.cn

Abstract. This paper examines an experimental setup of an organic Rankine cycle and proposes a method for describing it using differential equations. The aim of the work is to obtain approximate values of the setup's characteristics before conducting the experiment. The constructive scheme of the experimental device and its operating principle are described in detail. The power circuit of the setup is composed, and complex impedance, frequency function, amplitude-frequency, and phase-frequency characteristics are obtained based on the mathematical transformation of the circuit. The frequency response of the circuit is constructed. As a result of the calculations, the amplitude-frequency and phase-frequency characteristics are obtained, and graphs are plotted based on them. Conclusions are drawn about the dependence of the characteristics on the change in parameters, and the shape of the graphs is explained. The results of the work can be used to predict the behavior of the experimental setup of the organic Rankine cycle and optimize its parameters before conducting physical experiments.

Аннотация. Рассматривается экспериментальная установка органического цикла Ренкина и предлагается методика ее описания с помощью дифференциальных уравнений. Цель работы — получить приближенные значения характеристик установки до проведения эксперимента. Подробно описывается конструктивная схема экспериментального устройства и принцип его работы. Составлена энергетическая цепь установки, на основе математического преобразования которой получены комплексное сопротивление, частотная функция, амплитудно-частотная и фазочастотная характеристики. Построена частотная характеристика цепи. В результате расчетов получены амплитудно-частотная и фазочастотная характеристики, на основе которых построены графики. Сделаны выводы о зависимости характеристик от изменения параметров и объяснена форма графиков. Результаты работы могут быть использованы для прогнозирования поведения экспериментальной установки органического цикла Ренкина и оптимизации ее параметров перед проведением физических экспериментов.



Keywords: organic Rankine cycle, power circuit, frequency response, amplitude-frequency characteristic, phase-frequency characteristic, modeling.

Ключевые слова: органический цикл Ренкина, энергетическая цепь, частотная характеристика, амплитудно-частотная характеристика, фазочастотная характеристика, моделирование.

The study of hydraulics and heat transfer processes is crucial for understanding and optimizing various engineering systems. Mathematical modeling, particularly using differential equations, has been widely used to address this challenge. However, the complexity of hydraulic and heat transfer systems often requires a systematic approach to model development and analysis.

In recent years, the application of energy circuit theory to describe hydraulic and heat transfer processes has gained attention. Despite the growing interest in these methods, there is still a need for a comprehensive study that combines the energy circuit approach with differential equations and black-box modeling to describe hydraulic and heat transfer processes.

The novelty of this work lies in the integration of energy circuit theory, differential equations, and black-box modeling to create a unified framework for describing hydraulic and heat transfer processes. The proposed methodology involves building an energy circuit, compiling equations, setting input and output through the black box, calculating equations using the black box, writing equations for the image, compiling the complex resistance equation, distinguishing coefficients, writing the frequency function for the energy circuit, and distinguishing the real and imaginary parts of the complex resistance to calculate the amplitude-frequency and phase-frequency characteristics.

Material and methods of research

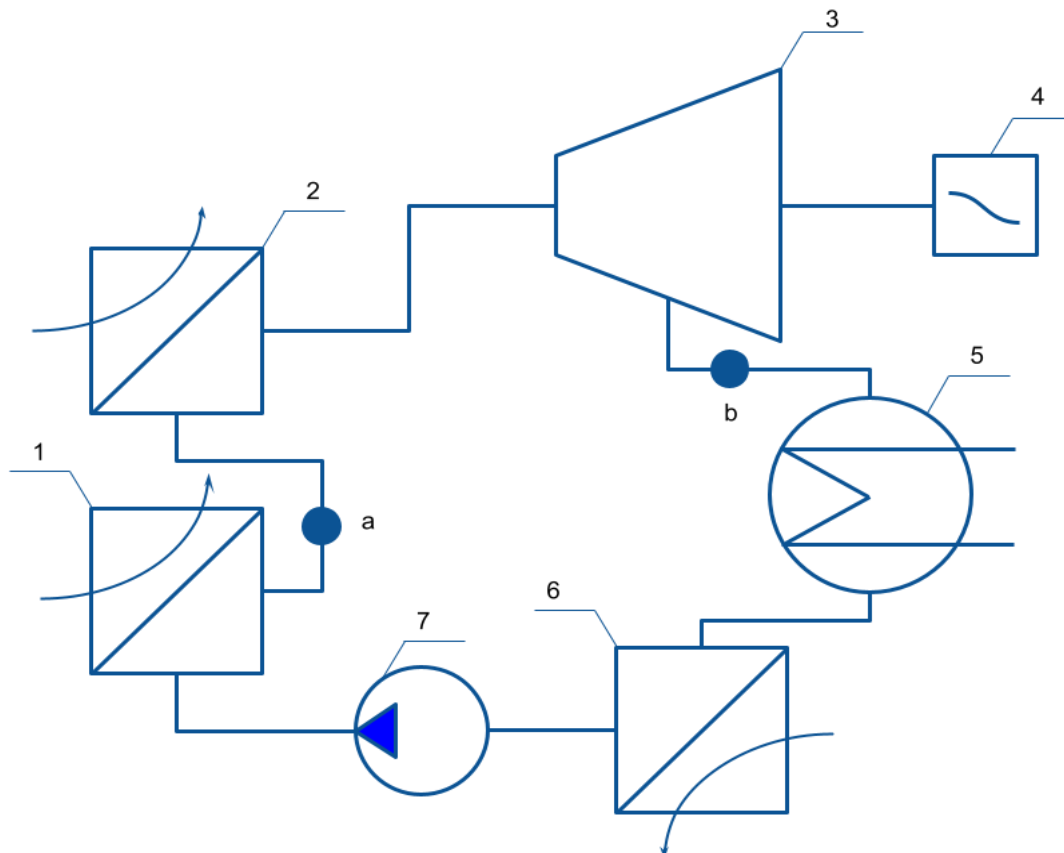


Figure 1. Experimental device for organic Rankine cycle

Table 1
SYMBOLS IN FIGURE 1

Position	Name
1	Evaporator
2	Superheater
3	Turbine
4	Generator
5	Condenser
6	Cooler
7	Pump

The principle of operation of the experimental setup

Figure 2 shows an experimental installation of a waste heat exchanger with a phase change.

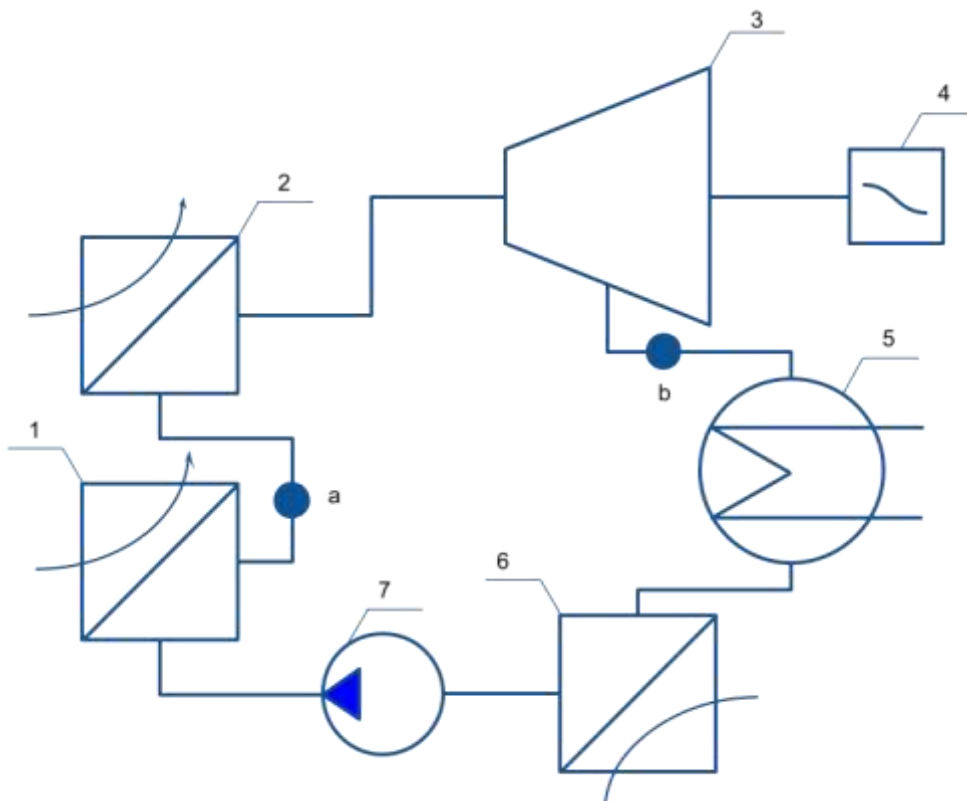


Figure 2. Experimental device for organic Rankine cycle: 1 – evaporator; 2 – superheater 3 – turbine; 4 – generator; 5 – condenser; 6 – cooler; 7 – pump

The working steam generated in the evaporator 1 reaches the turbine 3 through the superheater 2 for improving energy potential. After producing a work in the generator 4, low-potential gas make a phase change to the fluid in the condenser 5. After decreasing of temperature in the cooler 6, working fluid reaches to the pump 7. The heat transfer principle is shown in Figure 5.

In the course of the study, for a better understanding of the scheme, it was decided to study 2 characteristics of hydraulic and thermal, in order to better understand the nature of the forces arising and to more accurately determine the required parameters on the obtained model.

The first is hydraulic, which takes into account elastic properties of a spring with pliability l_1 (pliability is the inverse of elasticity), inertial properties of a liquid by mass m_1 , pressure losses in the pipeline by means of active resistance r_1 . The third part is the network pump, and elastic

properties of the spring with pliability l_1 (pliability is the value of the inverse elasticity) cylinder walls by active resistance.

In the first power circuit the hydraulic characteristics at the moment of closing of the shock valve is considered. This circuit contains 2 elements.

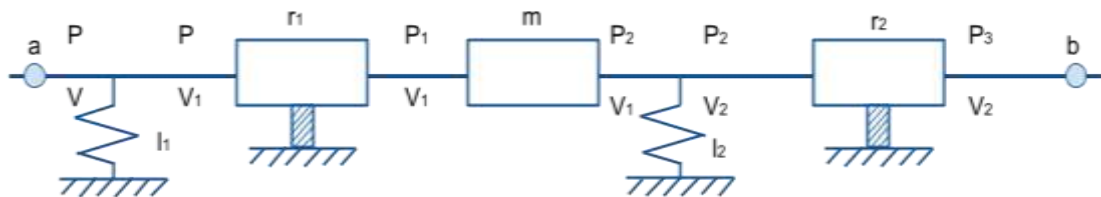


Figure 3. Hydraulic circuit

The circuit link equations:

$$\begin{cases} P = r_1 V_1^2 + m \dot{V}_1 + r_2 V_2^2 + P_3 \\ V = l_1 \dot{P} + l_2 \dot{P}_2 + V_2 \end{cases} \quad (1)$$

Black box:



Figure 4. Black box for hydraulic energy circuit

Equations for P_3, P_2, P_1 :

$$P_3 = P_{30} + \bar{P}_3 \quad (2)$$

$$P_2 = r_2 V_2^2 + P_3 \quad (3)$$

$$P_1 = m \dot{V}_1 + P_2 \quad (4)$$

Equations for V_2, V_1 :

$$V_2 = V_{20} + \bar{V}_2 \quad (5)$$

$$V_1 = l_2 \dot{\bar{P}}_2 + V_{20} + \bar{V}_2 \quad (6)$$

Equation for \dot{P}_2 :

$$\dot{P}_2 = r_2 V_2^2 + \dot{P}_3 = r_2 V_{20}^2 + 2r_2 V_{20} \bar{V}_2 + P_{30} + \bar{P}_3 \quad (7)$$

Equation for $\dot{\bar{P}}_2$:

$$\dot{\bar{P}}_2 = 2r_2 V_{20} \dot{\bar{V}}_2 + \dot{\bar{P}}_3 \quad (8)$$

Equation for V_1 :

$$V_1 = 2l_2 r_2 V_{20} \dot{\bar{V}}_2 + l_2 \dot{\bar{P}}_3 + V_{20} + \bar{V}_2 \quad (9)$$

Equation for $\dot{\bar{V}}_1$

$$\dot{\bar{V}}_1 = 2l_2r_2V_{20}\ddot{\bar{V}}_2 + l_2\ddot{\bar{P}}_3 + \dot{\bar{V}}_2 \quad (10)$$

Equation for V_1^2 :

$$V_1^2 = \left[V_{20} + (2l_2r_2V_{20}\dot{\bar{V}}_2 + l_2\dot{\bar{P}}_3 + \bar{V}_2) \right]^2 \approx V_{20}^2 + 2V_{20}(2l_2r_2V_{20}\dot{\bar{V}}_2 + l_2\dot{\bar{P}}_3 + \bar{V}_2) \quad (11)$$

Equation for V_2^2 :

$$V_2^2 = V_{20}^2 + 2V_{20}\bar{V}_2 + \bar{V}_2^2 \quad (12)$$

Equation for P :

$$\begin{aligned} P &= r_1(V_{20}^2 + 4V_{20}^2l_2r_2\dot{\bar{V}}_2 + 2V_{20}l_2\dot{\bar{P}}_3 + 2V_{20}\bar{V}_2) + m_1(2l_2r_2V_{20}\ddot{\bar{V}}_2 + l_2\ddot{\bar{P}}_3 + \dot{\bar{V}}_2) \\ &\quad + r_2(V_{20}^2 + 2V_{20}\bar{V}_2 + \bar{V}_2^2) + P_{30} + \bar{P}_3 \\ &= m_1l_2\ddot{\bar{P}}_3 + 2r_1l_2V_{20}\dot{\bar{P}}_3 + \bar{P}_3 + P_{30} + 2m_1l_2r_2V_{20}\ddot{\bar{V}}_2 + \dot{\bar{V}}_2(4l_2r_1r_2V_{20}^2 + m_1) \\ &\quad + \bar{V}_2(4r_2V_{20} + 2r_1V_{20}) + 2r_2V_{20}^2 + r_1V_{20}^2 \end{aligned} \quad (13)$$

Equation for images:

$$(a_1s^2 + a_2s + a_3)V_2(s) = -(b_1s^2 + b_2s^1 + b_3)P_3(s) \quad (14)$$

Coefficients:

$$\begin{aligned} a_1 &= m_1l_2 \\ a_2 &= 2r_1l_2V_{20} \\ a_3 &= 1 \\ b_1 &= 2m_1l_2r_2V_{20} \\ b_2 &= 4l_2r_1r_2V_{20}^2 + m_1 \\ b_3 &= 4r_2V_{20} + 2r_1V_{20} \end{aligned} \quad (15)$$

Complex circuit resistance $Z(s)$:

$$Z(s) = \frac{P_3(s)}{V_2(s)} = \frac{a_1s^2 + a_2s + a_3}{-b_1s^2 - b_2s - b_3} \quad (16)$$

Frequency function of the circuit:

$$s \rightarrow j\Omega, j^2 = -1 \quad (17)$$

Frequency function of the circuit:

$$\begin{aligned} z(j\Omega) &= \frac{-a_1\Omega^2 + a_2j\Omega + a_3}{b_1\Omega^2 - b_2j\Omega - b_3} = \frac{(-a_1\Omega^2 + a_2j\Omega + a_3) \cdot [(b_1\Omega^2 - b_3) + b_2j\Omega]}{[(b_1\Omega^2 - b_3) - b_2j\Omega] + [(b_1\Omega^2 - b_3) + b_2j\Omega]} \\ &= \frac{(-a_1b_1\Omega^4 + a_1b_3\Omega^2 - a_1b_2j\Omega^3 + a_2b_1j\Omega^3 - a_2b_3j\Omega - a_2b_2\Omega^2) + a_3b_1\Omega^2 - a_3b_3 + a_3b_2j\Omega}{(b_1\Omega^2 - b_3)^2 + b_2^2\Omega^2} \\ &= \frac{[-a_1b_1\Omega^4 + (a_2b_1 - a_1b_2)j\Omega^3 + (a_1b_3 - a_2b_2 + a_3b_1)\Omega^2] + (a_3b_2 - a_2b_3)j\Omega - a_3b_3}{(b_1\Omega^2 - b_3)^2 + b_2^2\Omega^2} \end{aligned} \quad (18)$$

The real part of the frequency function:

$$Re(j\Omega) = \frac{-a_1b_1\Omega^4 + (a_1b_3 - a_2b_2 + a_3b_1)\Omega^2 - a_3b_3}{(b_1\Omega^2 - b_3)^2 + b_2^2\Omega^2} \quad (19)$$



Imaginary part of the frequency function:

$$Im(j\Omega) = \frac{(a_2 b_1 - a_1 b_2)\Omega^3 + (a_3 b_2 - a_2 b_3)\Omega}{(b_1 \Omega^2 - b_3)^2 + b_2^2 \Omega^2} j \quad (20)$$

Amplitude-frequency response (frequency response) of the circuit:

$$A(j\Omega) = \sqrt{Re(j\Omega)^2 + Im(j\Omega)^2} \quad (21)$$

Phase frequency response (FFC) of the circuit:

$$\varphi(j\Omega) = -arctg \frac{Im(j\Omega)}{Re(j\Omega)} \quad (22)$$

Figure 5 shows the part of the installation where heat transfer takes place.

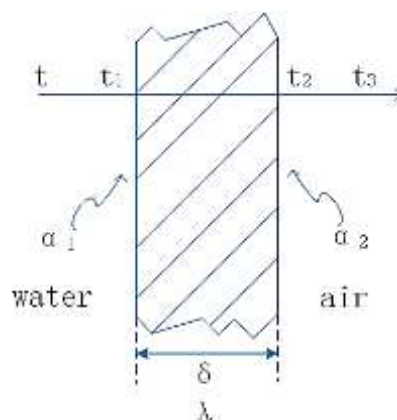


Figure 5. Part of the heat transfer plant: t - the temperature of hot water; t_1 , t_2 - wall temperature; t_3 - the temperature of the air; α_1 - convective heat transfer coefficient of water and left wall; α_2 - convective heat transfer coefficient of air and right wall; δ - the thickness of the wall surface; λ - Thermal conductivity of the wall

When the hot water flows, the convective heat transfer coefficient between the water and the left wall is h_1 , and the temperature of t is greater than t_1 , so the wall absorbs the heat brought by the hot water, and the wall temperature rises. When the temperature rises to t_1 , the surface temperature of the left wall is stable. The thickness of the wall is λ , and the heat is transmitted from the left wall to the right wall by means of heat conduction. When the temperature rises to t_2 , the surface temperature of the right wall reaches a stable state. The right wall carries out convective heat transfer with the air, and the convective heat transfer coefficient is h_2 . Through convective heat transfer, heat is transferred to the air until the air temperature t_3 reaches a stable state.

Calculate the convective heat transfer thermal resistance r_1 :

$$r_1 = \frac{1}{\alpha_1 F} \quad (23)$$

Calculate the convective heat transfer thermal resistance r_2 :

$$r_2 = \frac{\delta}{\lambda F} \quad (24)$$

Calculate the convective heat transfer thermal resistance r_3 :

$$r_3 = \frac{1}{\alpha_2 F} \quad (25)$$

Total thermal conductivity k.

$$k = \frac{1}{r_1 + r_2 + r_3} = \frac{1}{\frac{1}{\alpha_1 F} + \frac{\delta}{\lambda F} + \frac{1}{\alpha_2 F}} \quad (26)$$

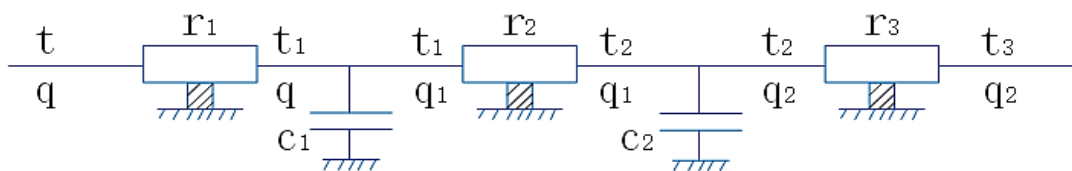


Figure 6. Heat transfer energy circuit

The circuit link equations:

$$\begin{cases} t = r_1 q + r_2 q_1 + r_3 q_2 + t_3 \\ q = c_1 \dot{t}_1 + c_2 \dot{t}_2 + q_2 \end{cases} \quad (27)$$

The input and output of the energy chain for thermal calculation are presented in the form of a “black” box.

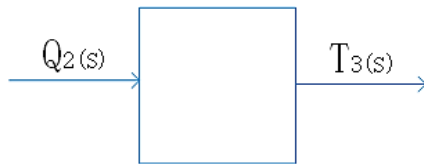


Figure 7. Black box for heat transfer

Equations for $t_3, t_2, \dot{t}_2, t_1, q_2$:

$$t_3 = t_{30} + \bar{t}_3 \quad (28)$$

$$t_2 = r_3 q_2 + t_3 \quad (29)$$

$$\dot{t}_2 = \dot{\bar{t}}_2 = r_3 \dot{q}_2 + \dot{\bar{t}}_3 \quad (30)$$

$$t_1 = r_2 q_1 + t_2 \quad (31)$$

$$q_2 = q_{20} + \bar{q}_2 \quad (32)$$

Equations on q_1 from the 1st link:

$$q_1 = c_2 \dot{t}_2 + q_2 = c_2(r_3 \dot{q}_2 + \dot{\bar{t}}_3) + q_{20} + \bar{q}_2 = c_2 r_3 \dot{q}_2 + c_2 \dot{\bar{t}}_3 + q_{20} + \bar{q}_2 \quad (33)$$

Equations on t_2 from the 1st link:

$$t_2 = r_3 q_2 + t_3 = r_3 q_{20} + r_3 \bar{q}_2 + t_{30} + \bar{t}_3 \quad (34)$$

The equation on t_1 :

$$\begin{aligned} t_1 &= r_2 q_1 + t_2 = r_2(c_2 r_3 \dot{\bar{q}}_2 + c_2 \dot{\bar{t}}_3 + q_{20} + \bar{q}_2) + (r_3 q_{20} + r_3 \bar{q}_2 + t_{30} + \bar{t}_3) \\ &= c_2 r_2 r_3 \dot{\bar{q}}_2 + c_2 r_2 \dot{\bar{t}}_3 + r_2 q_{20} + r_2 \bar{q}_2 + r_3 q_{20} + r_3 \bar{q}_2 + t_{30} + \bar{t}_3 \\ &= c_2 r_2 r_3 \dot{\bar{q}}_2 + (r_2 + r_3) \bar{q}_2 + (r_2 + r_3) q_{20} + c_2 r_2 \dot{\bar{t}}_3 + \bar{t}_3 + t_{30} \end{aligned} \quad (35)$$

The equation on $\dot{\bar{t}}_1$:

$$\dot{\bar{t}}_1 = c_2 r_2 r_3 \ddot{\bar{q}}_2 + (r_2 + r_3) \dot{\bar{q}}_2 + c_2 r_2 \ddot{\bar{t}}_2 + \dot{\bar{t}}_3 \quad (36)$$

The equation on q :

$$\begin{aligned} q &= c_1 \dot{t}_1 + c_2 \dot{t}_2 + q_2 \\ &= c_1 [c_2 r_2 r_3 \ddot{\bar{q}}_2 + (r_2 + r_3) \dot{\bar{q}}_2 + c_2 r_2 \ddot{\bar{t}}_2 + \dot{\bar{t}}_3] + c_2 (r_3 \dot{\bar{q}}_2 + \dot{\bar{t}}_3) \\ &\quad + (q_{20} + \bar{q}_2) \\ &= c_1 c_2 r_2 r_3 \ddot{\bar{q}}_2 + (c_1 r_2 + c_1 r_3 + c_2 r_3) \dot{\bar{q}}_2 + \bar{q}_2 + q_{20} + c_1 c_2 r_2 \ddot{\bar{t}}_2 \\ &\quad + (c_1 + c_2) \dot{\bar{t}}_3 \end{aligned} \quad (37)$$

The equation on t :

$$\begin{aligned} t &= r_1 q + r_2 q_1 + r_3 q_2 + t_3 \\ &= r_1 [c_1 c_2 r_2 r_3 \ddot{\bar{q}}_2 + (c_1 r_2 + c_1 r_3 + c_2 r_3) \dot{\bar{q}}_2 + \bar{q}_2 + q_{20} + c_1 c_2 r_2 \ddot{\bar{t}}_2 \\ &\quad + (c_1 + c_2) \dot{\bar{t}}_3] + r_2 (c_2 r_3 \dot{\bar{q}}_2 + c_2 \dot{\bar{t}}_3 + q_{20} + \bar{q}_2) + r_3 (q_{20} + \bar{q}_2) + t_{30} + \bar{t}_3 \\ &= [c_1 c_2 r_1 r_2 r_3 \ddot{\bar{q}}_2 + (c_1 r_1 r_2 + c_1 r_1 r_3 + c_2 r_1 r_3) \dot{\bar{q}}_2 + r_1 \bar{q}_2 + r_1 q_{20} + c_1 c_2 r_1 r_2 \ddot{\bar{t}}_2 \\ &\quad + (c_1 r_1 + c_2 r_1) \dot{\bar{t}}_3] + (c_2 r_2 r_3 \dot{\bar{q}}_2 + c_2 r_2 \dot{\bar{t}}_3 + r_2 q_{20} + r_2 \bar{q}_2) + (r_3 q_{20} + r_3 \bar{q}_2) \\ &\quad + t_{30} + \bar{t}_3 \\ &= c_1 c_2 r_1 r_2 r_3 \ddot{\bar{q}}_2 + (c_1 r_1 r_2 + c_1 r_1 r_3 + c_2 r_1 r_3 + c_2 r_2 r_3) \dot{\bar{q}}_2 + (r_1 + r_2 + r_3) \bar{q}_2 \\ &\quad + (r_1 + r_2 + r_3) q_{20} + c_1 c_2 r_1 r_2 \ddot{\bar{t}}_2 + (c_1 r_1 + c_2 r_1 + c_2 r_2) \dot{\bar{t}}_3 + \bar{t}_3 + t_{30} \\ &= b_1 \ddot{\bar{q}}_2 + b_2 \dot{\bar{q}}_2 + b_3 \bar{q}_2 + b_4 q_{20} + a_1 \ddot{\bar{t}}_2 + a_2 \dot{\bar{t}}_3 + a_3 \bar{t}_3 + a_4 t_{30} \end{aligned} \quad (38)$$

Equation for images:

$$(a_1 s^2 + a_2 s + a_3) T_3(s) = -(b_1 s^2 + b_2 s + b_3) Q_2(s) \quad (39)$$

Coefficients:

$$\begin{aligned} a_1 &= c_1 c_2 r_1 r_2 \\ a_2 &= c_1 r_1 + c_2 r_1 + c_2 r_2 \\ a_3 &= 1 \\ b_1 &= c_1 c_2 r_1 r_2 r_3 \\ b_2 &= c_1 r_1 r_2 + c_1 r_1 r_3 + c_2 r_1 r_3 + c_2 r_2 r_3 \\ b_3 &= r_1 + r_2 + r_3 \end{aligned} \quad (40)$$

Complex resistance $Z(s)$:

$$Z(s) = \frac{T_3(s)}{Q_2(s)} = \frac{-b_1 s^2 - b_2 s - b_3}{a_1 s^2 + a_2 s + a_3} \quad (41)$$

Frequency functions of the circuit:

$$s \rightarrow j\Omega, j^2 = -1 \quad (42)$$

Frequency function of the circuit:



$$\begin{aligned}
 Z(s) &= \frac{T_3(s)}{Q_2(s)} = \frac{-b_1 s^2 - b_2 s - b_3}{a_1 s^2 + a_2 s + a_3} = \frac{b_1 \Omega^2 - b_2 j\Omega - b_3}{-a_1 \Omega^2 + a_2 j\Omega + a_3} \\
 &= \frac{(b_1 \Omega^2 - b_2 j\Omega - b_3)[(-a_1 \Omega^2 + a_3) - a_2 j\Omega]}{[(-a_1 \Omega^2 + a_3) + a_2 j\Omega][(-a_1 \Omega^2 + a_3) - a_2 j\Omega]} \\
 &= \frac{\left(-a_1 b_1 \Omega^4 + a_3 b_1 \Omega^2 - a_2 b_1 j\Omega^3 + a_1 b_2 j\Omega^3 - a_3 b_2 j\Omega - a_2 b_2 \Omega^2 \right)}{(-a_1 \Omega^2 + a_3)^2 + a_2^2 \Omega^2} \\
 &+ a_1 b_3 \Omega^2 - a_3 b_3 + a_2 b_3 j\Omega \\
 &= \frac{\left[-a_1 b_1 \Omega^4 + (a_1 b_2 - a_2 b_1) j\Omega^3 + (a_3 b_1 - a_2 b_2 + a_1 b_3) \Omega^2 + \right]}{(-a_1 \Omega^2 + a_3)^2 + a_2^2 \Omega^2} \\
 &\quad \frac{(a_2 b_3 - a_3 b_2) j\Omega - a_3 b_3}{(-a_1 \Omega^2 + a_3)^2 + a_2^2 \Omega^2}
 \end{aligned} \tag{43}$$

We derive the real part of the complex resistance:

$$Re(j\Omega) = \frac{-a_1 b_1 \Omega^4 + (a_3 b_1 - a_2 b_2 + a_1 b_3) \Omega^2 - a_3 b_3}{(-a_1 \Omega^2 + a_3)^2 + a_2^2 \Omega^2} \tag{44}$$

We derive the imaginary part of the complex resistance:

$$Im(j\Omega) = \frac{(a_1 b_2 - a_2 b_1) \Omega^3 + (a_2 b_3 - a_3 b_2) \Omega}{(-a_1 \Omega^2 + a_3)^2 + a_2^2 \Omega^2} j \tag{45}$$

We obtain the amplitude-frequency function of the energy circuit:

$$A(j\Omega) = \sqrt{Re(j\Omega)^2 + Im(j\Omega)^2} \tag{46}$$

Get the phase-frequency function of the energy circuit:

$$\varphi(j\Omega) = -arctg \frac{Im(j\Omega)}{Re(j\Omega)} \tag{47}$$

Construction of frequency characteristics of the circuit when changing at least three parameters. The known conditions: P – pressure, kPa; V – volume flow, l/s [liter per second]; r_1 – active resistance, $\left[\frac{kPa \cdot s^2}{lit}\right]$; m_1 – mass of working fluid, [kg]; l_1, l_2 – hydraulic compliance, $\left[\frac{lit \cdot s}{Pa}\right]$, 1 litre = 10^{-3} metre.

Parameter are calculated or found from the experiment.

Are set by the input power of the circuit, for example $n_0 = 400$ W, as well as the inlet pressure $P_0 = 100$ kPa. Hire the pressure loss on the active resistance is assumed $5 \pm 10\%$.

$$V_0 = \frac{n_0}{P_0} = \frac{400}{100} = 4 \text{ l/s} \tag{48}$$

According to equation write the formula for r_1, r_2 :

$$r_1 = \frac{P - P_1}{V_0^2} = \frac{0.1 \times 100}{4^2} = 0.625 \left[\frac{kPa \cdot s^2}{lit} \right] \tag{49}$$

$$r_2 = \frac{P - P_2}{V_0^2} = \frac{0.2 \times 100}{4^2} = 1.25 \left[\frac{kPa \cdot s^2}{lit} \right] \tag{49}$$

The mass of working fluid depends on the volume of pipelines.

$$m_1 = 10 \text{ kg} \tag{50}$$



The compliance is found for equation:

$$l_1 = \frac{V - V_1}{\dot{P}} = \frac{0.1 \times 4}{0.5 \times 100} = 0.008 \left[\frac{\text{lit} \cdot \text{s}}{\text{kPa}} \right] \quad (51)$$

$$l_1 = l_2 = 0.008 \left[\frac{\text{lit} \cdot \text{s}}{\text{kPa}} \right] \quad (52)$$

Algorithm for plotting graphs.

The values of the coefficients are calculated:

$$\begin{aligned} a_1 &= m_1 l_2 = 10 \times 0.008 = 0.08 \\ a_2 &= 2r_1 l_2 V_{20} = 2 \times 0.625 \times 0.008 \times 4 = 0.04\Omega \\ a_3 &= 1 \\ b_1 &= 2m_1 l_2 r_2 V_{20} = 2 \times 10 \times 0.008 \times 1.25 \times 4 = 0.8 \\ b_2 &= 4l_2 r_1 r_2 V_{20}^2 + m_1 = 4 \times 0.008 \times 0.625 \times 1.25 \times 16 = 0.4 \\ b_3 &= 4r_2 V_{20} + 2r_1 V_{20} = 4 \times 1.25 \times 4 + 2 \times 0.625 \times 4 = 25 \end{aligned} \quad (53)$$

The limit of change Ω is accept, $\Omega = 1 \dots 10 \text{ rad/s}$. Calculation of the real and imaginary part of the frequency function: $\Omega = 1 \text{ rad/s}$

$$\begin{aligned} Re(1) &= \frac{-a_1 b_1 \Omega^4 + (a_1 b_3 - a_2 b_2 + a_3 b_1) \Omega^2 - a_3 b_3}{(b_1 \Omega^2 - b_3)^2 + b_2^2 \Omega^2} \quad (54) \\ &= \frac{\left[-0.08 \times 0.8 \times 1^4 + \left(\frac{0.08 \times 25 - 0.04 \times 0.4}{1 \times 0.8} + \right) \times 1^2 \right]}{(0.8 \times 1^2 - 25)^2 + 0.4^2 \times 1^2} \\ &= -0.038033 \end{aligned}$$

$$\begin{aligned} Im(1) &= \frac{(a_2 b_1 - a_1 b_2) \Omega^3 + (a_3 b_2 - a_2 b_3) \Omega}{(b_1 \Omega^2 - b_3)^2 + b_2^2 \Omega^2} j \quad (55) \\ &= \frac{\left[(0.04 \times 0.8 - 0.08 \times 0.4) \times 1^3 + \left(\frac{1 \times 0.4}{-0.04 \times 0.25} \right) \times 1 \right]}{(0.8 \times 1^2 - 25)^2 + 0.4^2 \times 1^2} \\ &= -0.001024 \end{aligned}$$

$$A(1) = \sqrt{Re(1)^2 + Im(1)^2} = \sqrt{(-0.038033)^2 + (-0.001024)^2} = 0.038047 \quad (56)$$

$$\varphi(1) = -\arctg \frac{Im(1)}{Re(1)} = -\arctg \frac{-0.001024}{-0.038033} = -0.026923 \quad (57)$$

According to equation write the formula for

CIRCUIT PARAMETERS

Table 2

m_1, kg	$r_1, \left[\frac{\text{kPa} \cdot \text{s}^2}{\text{lit}} \right]$	$l_1, \left[\frac{\text{lit} \cdot \text{s}}{\text{Pa}} \right]$	$l_2, \left[\frac{\text{lit} \cdot \text{s}}{\text{Pa}} \right]$	P_{30}, kPa	$V_{30}, \text{lit/s}$
10	0.625	0.008	0.008	100	4
10	0.625	0.008	0.016	100	4
10	0.625	0.008	0.024	100	4



Dependency graphs are plotted based on the input values. For the best perception of graphs values are taken only those that affect the dependence. The values obtained for the first stage of the energy circuit are shown in Table 2.

Table 3
 RECEIVED INFORMATION FOR HYDRAULIC

Ω	$Aj\Omega_1$	$\varphi j\Omega_1$	$Aj\Omega_2$	$\varphi j\Omega_2$	$Aj\Omega_3$	$\varphi j\Omega_3$
1	0,038047	0,026923	0,036039	0,060777	0,033997	0,103554
2	0,031387	0,080428	0,021102	0,332414	0,015611	1,251047
3	0,017075	0,337578	0,046116	-0,722008	0,245282	-1,114882
4	0,026209	-0,649549	0,489127	1,183127	0,202355	0,176537
5	0,189373	-0,577902	0,194957	0,128051	0,141813	0,050349
6	0,421689	0,436343	0,145187	0,045688	0,124131	0,022767
7	0,202674	0,099087	0,127818	0,022798	0,116076	0,012556
8	0,156562	0,044021	0,119259	0,013346	0,111603	0,007759
9	0,137424	0,024608	0,114277	0,008597	0,108820	0,005167
10	0,127145	0,015519	0,111074	0,005907	0,106956	0,003629

Based on the results of the calculation, the graphs of the amplitude frequency response and phase-frequency response and frequency response of the circuit are constructed. Further in these graphs are under construction:

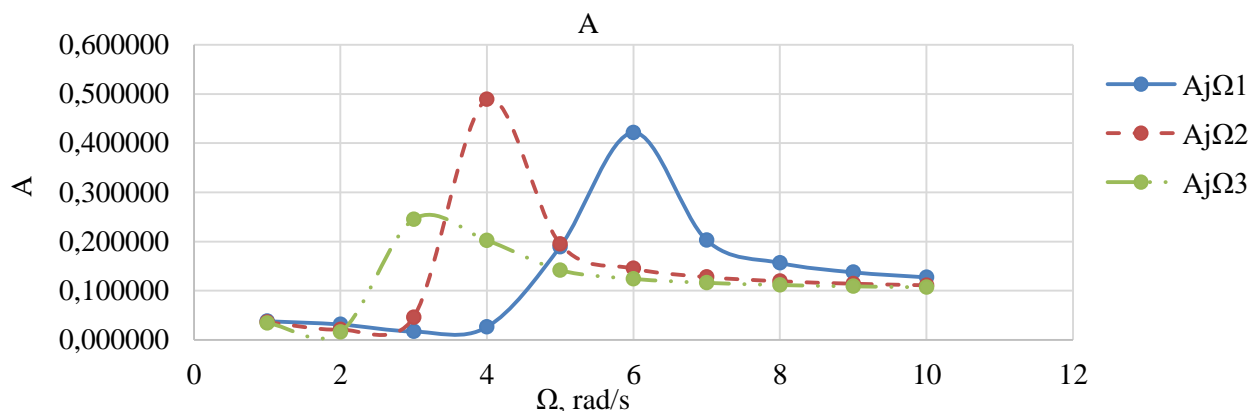


Figure 8. Amplitude frequency response

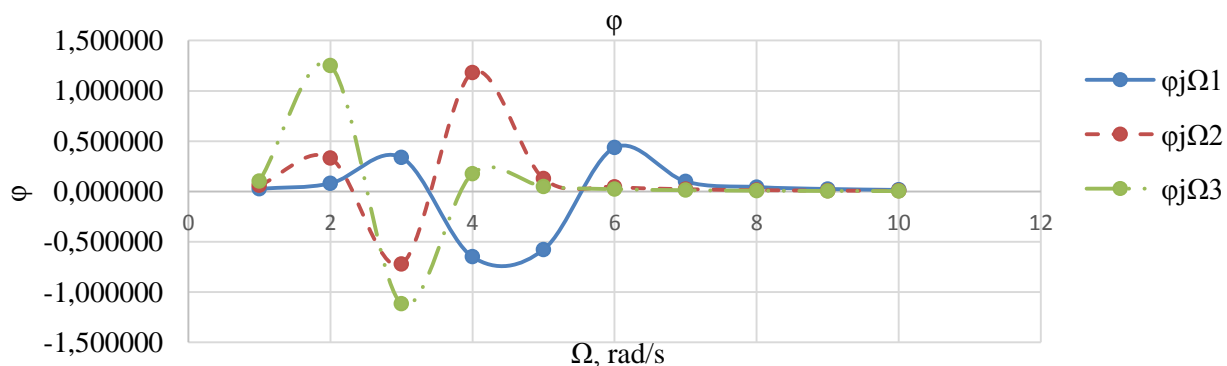


Figure 9. Phase frequency response

The graphs show a rapid increase in the amplitude A and phase-frequency characteristics φ of the circuit with increasing cyclic frequency Ω from 1 to 6, after which their smooth decay occurs.

For power circuits of the heat transfer calculations are conducted similarly and are written in table 3. A graphical view is presented in graphs 6-7.

The known conditions:

$$n_0 = 400W \quad (58)$$

$$r_1 = \frac{1}{\alpha_1 F} = \frac{1}{80 \times 2} = 6.25 \times 10^{-3} \left[\frac{kPa \cdot s^2}{lit} \right] \quad (59)$$

$$r_2 = \frac{\delta}{\lambda F} = \frac{0.002}{350 \times 2} = 2.86 \times 10^{-6} \left[\frac{kPa \cdot s^2}{lit} \right] \quad (60)$$

$$r_3 = \frac{1}{\alpha_2 F} = \frac{1}{120 \times 2} = 4.17 \times 10^{-3} \left[\frac{kPa \cdot s^2}{lit} \right] \quad (61)$$

$$q_0 = \frac{n_0}{t_0} = \frac{400}{100} = 4 \left[\frac{W}{^\circ C} \right]$$

$$c_1 = \frac{\Delta q}{t} = \frac{q - q_1}{t} = \frac{0.1 \times 4}{0.5 \times 100} = 0.008 \left[\frac{l}{s \cdot ^\circ C} \right] \quad (62)$$

$$c_2 = c_1 = 0.008 \left[\frac{l}{s \cdot ^\circ C} \right] \quad (63)$$

Algorithm for plotting graphs.

The values of the coefficients are calculated:

$$a_1 = c_1 c_2 r_1 r_2 = 0.008 \times 0.008 \times 6.25 \times 10^{-3} \times 2.86 \times 10^{-6} = 1.145 \times 10^{-12} \quad (64)$$

$$\begin{aligned} a_2 &= c_1 r_1 + c_2 r_1 + c_2 r_2 \\ &= 0.008 \times 6.25 \times 10^{-3} + 0.008 \times 6.25 \times 10^{-3} + 0.008 \times 2.86 \\ &\times 10^{-6} = 1 \times 10^{-4} \end{aligned}$$

$$a_3 = 1$$

$$\begin{aligned} b_1 &= c_1 c_2 r_1 r_2 r_3 = 0.008 \times 0.008 \times 6.25 \times 10^{-3} \times 2.86 \times 10^{-6} \times 4.17 \times 10^{-3} \\ &= 4.774 \times 10^{-15} \end{aligned}$$

$$\begin{aligned} b_2 &= c_1 r_1 r_2 + c_1 r_1 r_3 + c_2 r_1 r_3 + c_2 r_2 r_3 \\ &= 0.008 \times 6.25 \times 10^{-3} \times 2.86 \times 10^{-6} + 0.008 \times 6.25 \times 10^{-3} \\ &\times 4.17 \times 10^{-3} + 0.008 \times 6.25 \times 10^{-3} \times 4.17 \times 10^{-3} + 0.008 \\ &\times 2.86 \times 10^{-6} \times 4.17 \times 10^{-3} = 4.174 \times 10^{-7} \end{aligned}$$

$$b_3 = r_1 + r_2 + r_3 = 6.25 \times 10^{-3} + 2.86 \times 10^{-6} + 4.17 \times 10^{-3} = 1 \times 10^{-2}$$

The limit of change Ω is accept, $\Omega = 1 \dots 10$ rad/s. Calculation of the real and imaginary part of the frequency function: $\Omega = 1$ rad/s

$$\begin{aligned} Re(1) &= \frac{-a_1 b_1 \Omega^4 + (a_3 b_1 - a_2 b_2 + a_1 b_3) \Omega^2 - a_3 b_3}{(-a_1 \Omega^2 + a_3)^2 + a_2^2 \Omega^2} \quad (65) \\ &= \frac{-1.145 \times 10^{-12} \times 4.774 \times 10^{-15} \times 1^4 +}{\left(1 \times 4.774 \times 10^{-15} - 1 \times 10^{-4} \times 4.174 \times 10^{-7} \right) \times 1^2} \\ &= \frac{-1.145 \times 10^{-12} \times 1 \times 10^{-2}}{\left[(-1.145 \times 10^{-12} \times 1^2 + 1)^2 + (1 \times 10^{-4})^2 \times 1^2 \right]} \\ &= -0.010425 \end{aligned}$$



$$\begin{aligned}
 Im(1) &= \frac{(a_1 b_2 - a_2 b_1) \Omega^3 + (a_2 b_3 - a_3 b_2) \Omega}{(-a_1 \Omega^2 + a_3)^2 + a_2^2 \Omega^2} j \\
 &= \frac{\left[\begin{array}{l} (1.145 \times 10^{-12} \times 4.174 \times 10^{-7}) \times 1^3 \\ -1 \times 10^{-4} \times 4.774 \times 10^{-15} \end{array} \right] \times 1^3}{\left[\begin{array}{l} (1 \times 10^{-4} \times 1 \times 10^{-2}) \\ -1 \times 4.174 \times 10^{-7} \end{array} \right] \times 1} \\
 &= \frac{[(-1.145 \times 10^{-12} \times 1^2 + 1)^2 + (1 \times 10^{-4})^2 \times 1^2]}{6.255 \times 10^{-7}} \\
 &= 6.255 \times 10^{-7}
 \end{aligned} \tag{66}$$

$$A(1) = \sqrt{Re(1)^2 + Im(1)^2} = \sqrt{(-0.010425)^2 + (6.256 \times 10^{-7})^2} = 0.010425 \tag{67}$$

$$\varphi(1) = -arctg \frac{Im(1)}{Re(1)} = -arctg \frac{6.256 \times 10^{-7}}{-0.010425} = 5.99995 \times 10^{-5} \tag{68}$$

According to equation write the formula for

Table 4
 RECEIVED INFORMATION FOR HEAT TRANSFER

$r_1, \left[\frac{kPa \cdot s^2}{lit} \right]$	$r_2, \left[\frac{kPa \cdot s^2}{lit} \right]$	$r_3, \left[\frac{kPa \cdot s^2}{lit} \right]$	$c_1, \left[\frac{l}{s \cdot ^\circ C} \right]$	$c_2, \left[\frac{l}{s \cdot ^\circ C} \right]$
0.006251	2.86×10^{-6}	4.17×10^{-3}	0.008	0.008
0.06251	2.86×10^{-6}	4.17×10^{-3}	0.008	0.008
0.006251	2.86×10^{-6}	4.17×10^{-3}	0.08	0.08

The dependency graph is drawn based on input values. For optimal graph perception, take only those values that affect dependencies. The obtained values for the first stage of heat transfer are shown in Table 4.

Table 5
 VALUE AMPLITUDE FREQUENCY RESPONSE FOR ENERGY CIRCUIT

Ω	$Aj\Omega 1$	$\varphi j\Omega 1$	$Aj\Omega 2$	$\varphi j\Omega 2$	$Aj\Omega 3$	$\varphi j\Omega 3$
1	0,010425	5,99995E-05	0,066684	9,37601E-04	0,010425	1,19999E-04
2	0,010425	1,19999E-04	0,066684	1,87520E-03	0,010425	2,39998E-04
3	0,010425	1,79998E-04	0,066684	2,81279E-03	0,010425	3,59997E-04
4	0,010425	2,39998E-04	0,066683	3,75038E-03	0,010425	4,79996E-04
5	0,010425	2,99997E-04	0,066683	4,68796E-03	0,010425	5,99994E-04
6	0,010425	3,59997E-04	0,066683	5,62553E-03	0,010425	7,19993E-04
7	0,010425	4,19996E-04	0,066682	6,56309E-03	0,010425	8,39992E-04
8	0,010425	4,79996E-04	0,066682	7,50064E-03	0,010425	9,59990E-04
9	0,010425	5,39995E-04	0,066681	8,43817E-03	0,010425	1,07999E-03
10	0,010425	5,99994E-04	0,066681	9,37568E-03	0,010425	1,19999E-03

From the power loop heat transfer simulation plots, it can be observed that the amplitude-frequency response of the hydraulic loop A does not change with increasing cyclic frequency Ω , while the phase-frequency response φ increases in direct proportion to its increase.



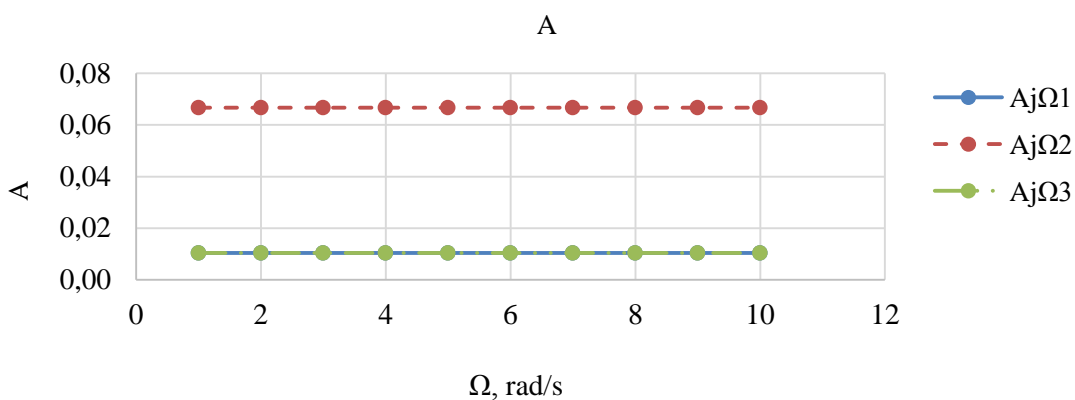


Figure 10. Amplitude frequency response

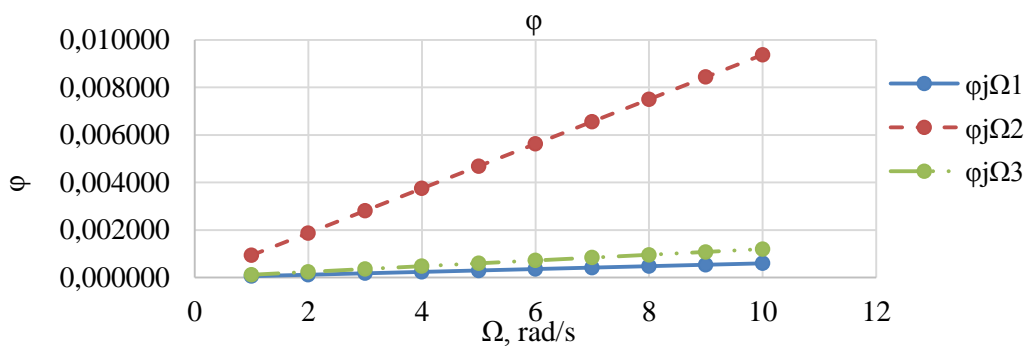


Figure 11. Phase frequency response

Results and Discussion

The main results obtained from this work are as follows:

A constructive scheme of the experimental setup for the organic Rankine cycle is proposed, and its operating principle is described in detail. The energy circuit of the setup is composed.

Complex impedance, frequency function, amplitude-frequency, and phase-frequency characteristics are obtained through mathematical transformation of the energy circuit. The frequency response of the circuit is constructed.

Modeling of the hydraulic and thermal circuits of the experimental setup is carried out based on the theory of energy circuits.

In the process of modeling the hydraulic energy circuit, it is found that there is a rapid increase in the amplitude-frequency and phase-frequency characteristics of the circuit with increasing cyclic frequency Ω , followed by a smooth decay.

When modeling the heat transfer energy circuit, it is established that the amplitude-frequency response of the hydraulic circuit does not change with increasing cyclic frequency Ω , while the phase-frequency response increases in direct proportion to its increase.

Based on the calculations performed, it is concluded that for the considered scheme of the organic Rankine cycle, the best variant of circuit parameters will be the one in which the hydraulic compliance l_2 is twice higher than the initial l_1 , the cyclic frequency Ω is equal to 4 rad/s, and the active resistance r_1 is the largest compared to other calculation variants of r_1 .

The obtained results are important for predicting the behavior of the experimental setup of the organic Rankine cycle and optimizing its parameters before conducting physical experiments. The proposed approach and modeling methodology have practical value for the analysis and design of similar energy systems.

Conclusion

In summary, this work presents a novel and comprehensive approach to modeling and analyzing hydraulic and heat transfer processes using energy circuit theory, differential equations, and black-box modeling. The proposed methodology integrates these techniques into a unified framework, providing a systematic approach to model development and analysis.

The results obtained from the modeling of the hydraulic and heat transfer energy circuits provide valuable insights into the behavior of the experimental setup of the organic Rankine cycle. The conclusions drawn from the calculations can be used to optimize the circuit parameters and predict the system's performance before conducting physical experiments.

The practical significance of this work lies in its potential to enhance the design and optimization of energy systems involving hydraulic and heat transfer processes. The proposed approach and methodology can be applied to similar systems, facilitating their analysis and improvement.

Further research could focus on validating the model through experimental studies and extending the methodology to other types of energy systems. Additionally, the integration of advanced optimization techniques with the proposed framework could lead to more efficient design and operation of hydraulic and heat transfer systems.

Acknowledgements: Kudashev Sergei Fedorovich, Zhang Qiang and Levtshev Alexey Pavlovich for assistance in conducting the research and organizing the article.

References:

1. Gogate, P. R., & Pandit, A. B. (2005). A review and assessment of hydrodynamic cavitation as a technology for the future. *Ultrasonics sonochemistry*, 12(1-2), 21-27. <https://doi.org/10.1016/j.ulsonch.2004.03.007>
2. Hammitt, F. G. (1980). Cavitation and multiphase flow phenomena.
3. Sivakumar, M., & Pandit, A. B. (2002). Wastewater treatment: a novel energy efficient hydrodynamic cavitation technique. *Ultrasonics sonochemistry*, 9(3), 123-131. [https://doi.org/10.1016/S1350-4177\(01\)00122-5](https://doi.org/10.1016/S1350-4177(01)00122-5)
4. Jeong, J. H., & Kwon, Y. C. (2006). Effects of ultrasonic vibration on subcooled pool boiling critical heat flux. *Heat and mass transfer*, 42, 1155-1161. <https://doi.org/10.1007/s00231-005-0079-1>
5. Wang, G., Senocak, I., Shyy, W., Ikohagi, T., & Cao, S. (2001). Dynamics of attached turbulent cavitating flows. *Progress in Aerospace sciences*, 37(6), 551-581. [https://doi.org/10.1016/S0376-0421\(01\)00014-8](https://doi.org/10.1016/S0376-0421(01)00014-8)
6. Barber, B. P., & Puttermann, S. J. (1991). Observation of synchronous picosecond sonoluminescence. *Nature*, 352(6333), 318-320. <https://doi.org/10.1038/352318a0>
7. Mason, T. J. (1988). Theory. Applications and uses of ultrasound in chemistry. *Sonochemistry*.
8. Suslick, K. S. (1991). The sonochemical hot spot. *The Journal of the Acoustical Society of America*, 89(4B_Supplement), 1885-1886. <https://doi.org/10.1121/1.2029381>
9. Misik, V., & Riesz, P. (1994). Free radical formation by ultrasound in organic liquids: a spin trapping and EPR study. *The Journal of Physical Chemistry*, 98(6), 1634-1640. <https://doi.org/10.1021/j100057a016>
10. Kumar, P. S., & Pandit, A. B. (1999). Modeling hydrodynamic cavitation. *Chemical engineering & technology: industrial chemistry-plant equipment-process engineering*-

- biotechnology, 22(12), 1017-1027. [https://doi.org/10.1002/\(SICI\)1521-4125\(199912\)22:12<1017::AID-CEAT1017>3.0.CO;2-L](https://doi.org/10.1002/(SICI)1521-4125(199912)22:12<1017::AID-CEAT1017>3.0.CO;2-L)
11. Chzhan, Yui, Li, Yumin & Tszi, Tszyan'bin (2011). Chislennoe modelirovaniye gidravlicheskogo kavitatsionnogo ustroistva s diafragmoi, 27(3), 219-223. (in Chinese)
12. Badve, M. P., Alpar, T., Pandit, A. B., Gogate, P. R., & Csoka, L. (2015). Modeling the shear rate and pressure drop in a hydrodynamic cavitation reactor with experimental validation based on KI decomposition studies. *Ultrasonics sonochemistry*, 22, 272-277. <https://doi.org/10.1016/j.ulsonch.2014.05.017>
13. Makeev, A. N. Impul'snaya sistema teplosnabzheniya obshchestvennogo zdaniya: avtoref. dis. ... kand.tekhn. nauk. Penza, 2010. 19 s. (in Russian)
14. Levtshev, A. P., Kudashev, S. F., Makeev, A. N., & Lysyakov, A. I. (2014). Vliyanie impul'snogo rezhima techeniya teplonositelya na koefitsient teploperedachi v plastinchatom teploobmennike sistemy goryachego vodosnabzheniya. *Sovremennye problemy nauki i obrazovaniya*, (2), 89-89. (in Russian)
15. Levtshev, A. P., Makeev, A. N., Makeev, N. F., Narvatov, Ya. A., & Golyanin, A. A. (2015). Obzor i analiz osnovnykh konstruktsii udarnykh klapanov dlya sozdaniya hidravlicheskogo udara. *Sovremennye problemy nauki i obrazovaniya*, (2-2), 188-188. (in Russian)
16. Aleksandrov, A. A., & Grigor'ev, B. A. (1999). Tablitsy teplofizicheskikh svoistv vody i vodyanogo para. Moscow. (in Russian)

Список литературы:

1. Gogate P. R., Pandit A. B. A review and assessment of hydrodynamic cavitation as a technology for the future // Ultrasonics sonochemistry. 2005. V. 12. №1-2. P. 21-27. <https://doi.org/10.1016/j.ulsonch.2004.03.007>
2. Hammitt F. G. Cavitation and multiphase flow phenomena. 1980.
3. Sivakumar M., Pandit A. B. Wastewater treatment: a novel energy efficient hydrodynamic cavitation technique // Ultrasonics sonochemistry. 2002. V. 9. №3. P. 123-131. [https://doi.org/10.1016/S1350-4177\(01\)00122-5](https://doi.org/10.1016/S1350-4177(01)00122-5)
4. Jeong J. H., Kwon Y. C. Effects of ultrasonic vibration on subcooled pool boiling critical heat flux // Heat and mass transfer. 2006. V. 42. P. 1155-1161. <https://doi.org/10.1007/s00231-005-0079-1>
5. Wang G., Senocak I., Shyy W., Ikohagi T., Cao S. Dynamics of attached turbulent cavitating flows // Progress in Aerospace sciences. 2001. V. 37. №6. P. 551-581. [https://doi.org/10.1016/S0376-0421\(01\)00014-8](https://doi.org/10.1016/S0376-0421(01)00014-8)
6. Barber B. P., Puterman S. J. Observation of synchronous picosecond sonoluminescence // Nature. 1991. V. 352. №6333. P. 318-320. <https://doi.org/10.1038/352318a0>
7. Mason T. J. Theory. Applications and uses of ultrasound in chemistry // Sonochemistry. 1988.
8. Suslick K. S. The sonochemical hot spot // The Journal of the Acoustical Society of America. 1991. V. 89. №4B_Supplement. P. 1885-1886. <https://doi.org/10.1121/1.2029381>
9. Misik V., Riesz P. Free radical formation by ultrasound in organic liquids: a spin trapping and EPR study // The Journal of Physical Chemistry. 1994. V. 98. №6. P. 1634-1640. <https://doi.org/10.1021/j100057a016>
10. Kumar P. S., Pandit A. B. Modeling hydrodynamic cavitation // Chemical engineering & technology: industrial chemistry-plant equipment-process engineering-biotechnology. 1999. V. 22. №12. P. 1017-1027. [https://doi.org/10.1002/\(SICI\)1521-4125\(199912\)22:12<1017::AID-CEAT1017>3.0.CO;2-L](https://doi.org/10.1002/(SICI)1521-4125(199912)22:12<1017::AID-CEAT1017>3.0.CO;2-L)



11. 章昱, 李育敏, 计建炳. 孔板水力空化装置的数值模拟 //化学反应工程与工艺. 2011. V. 27. №3. P. 219-223. (in Chinese)
12. Badve M. P., Alpar,T., Pandit A. B., Gogate P. R., Csoka L. Modeling the shear rate and pressure drop in a hydrodynamic cavitation reactor with experimental validation based on KI decomposition studies // Ultrasonics sonochemistry. 2015. V. 22. P. 272-277. <https://doi.org/10.1016/j.ulsonch.2014.05.017>
13. Макеев А. Н. Импульсная система теплоснабжения общественного здания: автореф. дис. ... канд.техн. наук. Пенза, 2010. 19 с.
14. Левцев А. П., Кудашев С. Ф., Макеев А. Н., Лысяков А. И. Влияние импульсного режима течения теплоносителя на коэффициент теплопередачи в пластинчатом теплообменнике системы горячего водоснабжения // Современные проблемы науки и образования. 2014. №2. С. 89-89.
15. Левцев А. П., Макеев А. Н., Макеев Н. Ф., Нарватов Я. А., Голянин А. А. Обзор и анализ основных конструкций ударных клапанов для создания гидравлического удара //Современные проблемы науки и образования. 2015. №2-2. С. 188-188.
16. Александров А. А., Григорьев Б. А. Таблицы теплофизических свойств воды и водяного пара. М.: Изд-во МЭИ, 1999. 158 с.

Работа поступила
в редакцию 15.05.2024 г.

Принята к публикации
24.05.2024 г.

Ссылка для цитирования:

Kireev N., Kudashev S., Zhang Qiang Modeling of the Organic Rankine Cycle Based on the Theory of Energy Chains // Бюллетень науки и практики. 2024. Т. 10. №6. С. 405-421. <https://doi.org/10.33619/2414-2948/103/43>

Cite as (APA):

Kireev, N., Kudashev, S., & Zhang Qiang (2024). Modeling of the Organic Rankine Cycle Based on the Theory of Energy Chains. *Bulletin of Science and Practice*, 10(6), 405-421. <https://doi.org/10.33619/2414-2948/103/43>

